## Supporting information

# Controlled Asymmetric Lamellar Nano-Morphology Obtained Through Nitroxide-Mediated Polymerization-Induced Microphase Separation

*Laura García Andújar,[1,†] Anne-Laure Brocas,[2] Sylvain Bourrigaud,[2,‡] Sylvie Cazaumayou,[2] Christophe Derail,[1] Maud Save, [1] Laurent Rubatat [1,*]*

[1] Universite de Pau et des Pays de l'Adour, E2S UPPA, CNRS, IPREM, Pau, France
[2] GRL, Arkema, B.P. 34, 64170 Lacq, France

**Present addresses**
[†] Saint Gobain Recherche Paris Quai Lucien Lefranc, 93303 Aubervilliers Cedex, France
[‡] M2i, Chemstart'up pôle 2, Allée Le Corbusier, 64170 Lacq, France

## 1. Molar and weight fractions in *s*-P(*n*BA-*co*-S)-SG1 and *s*-BCP_TBCP samples

The weight fraction ($W_x$, $W_y$, $W_z$, Eq S1) of each polymer moiety ($x$ = PMMA, $y$ = PS, $z$ = P*n*BA) in all copolymers of the present work were calculated from the molar fraction ($F_x$, $F_y$, $F_z$, Eq S2) of each copolymer calculated from the integrals of the respective moieties in the $^1$H NMR spectrum.

$$W_x = \frac{F_x \times M_x}{F_x \times M_x + F_y \times M_y + F_z \times M_z} \qquad \textbf{Eq S1.}$$

$$F_x = \frac{I_x}{I_x + I_y + I_z} \qquad \textbf{Eq S2.}$$

See note of Table S2 for the definition of $I_x$, $I_y$, $I_z$.

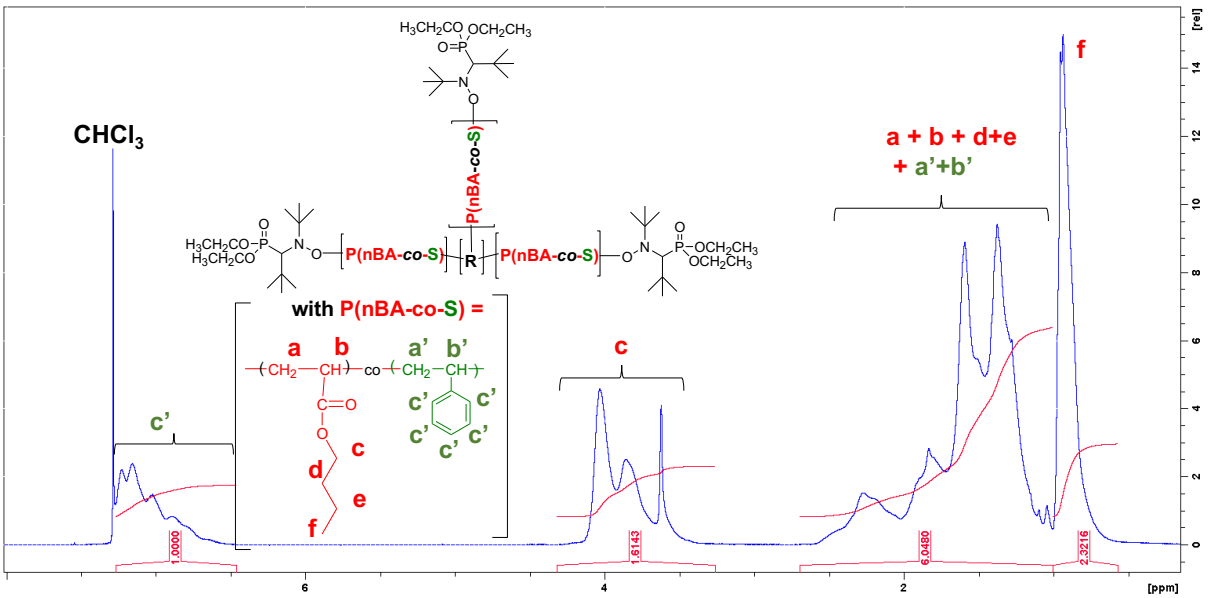


**Figure S1**. $^1$H NMR spectrum in $CDCl_3$ of *s*-P(*n*BA-*co*-S)-SG1 macroalkoxyamine used to determine its weight composition, i.e., 81 wt-% in *n*BA and 19 wt-% in S.

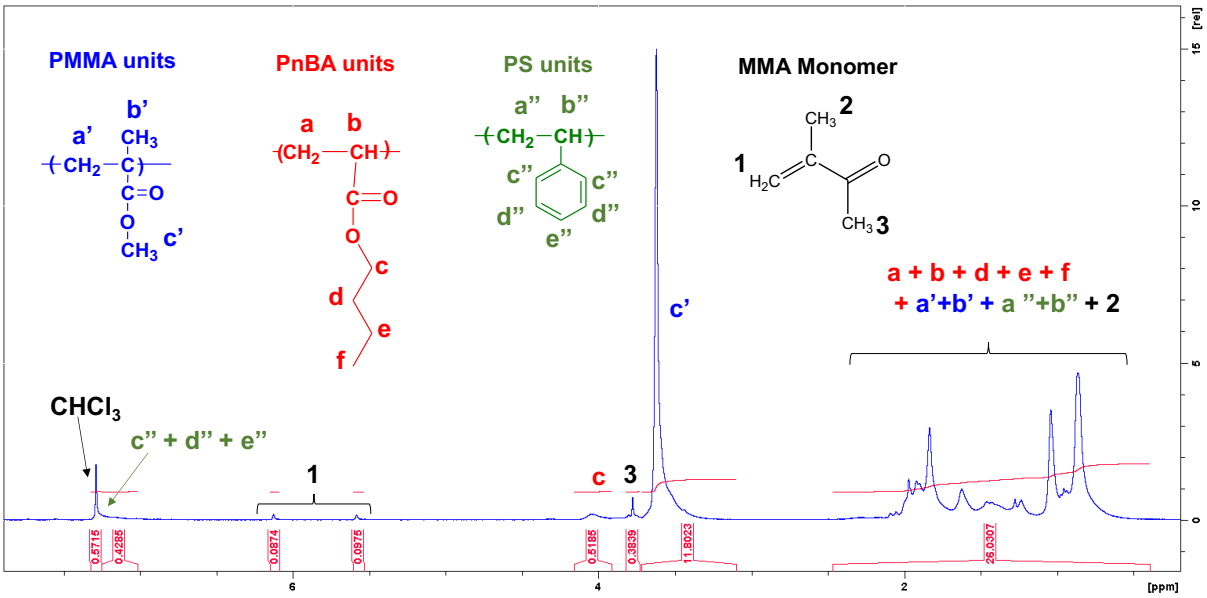


**Figure S2**. $^{1}$H NMR spectrum in $CDCl_3$ of *s*-$BCP_{95\%}$_$TBCP_{5\%}$ sample (see extracted values in Table 1 and Table S2).

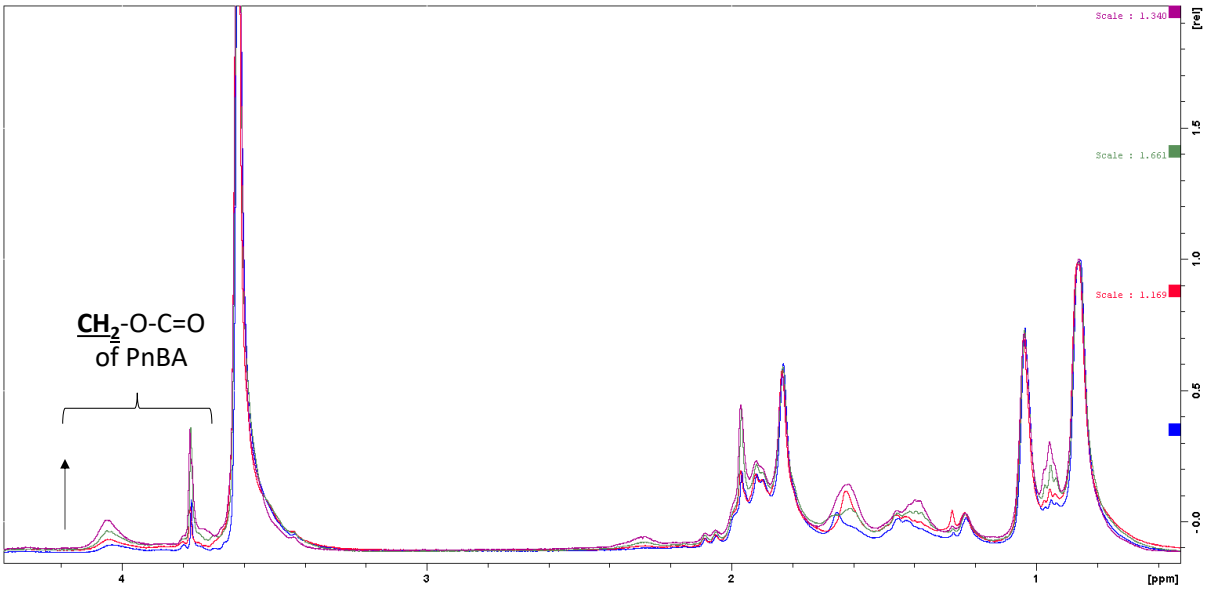


**Figure S3.** Overlay of $^{1}$H NMR spectrum in $CDCl_3$ of *s*-$BCP_{97.5\%}$_$TBCP_{2.5\%}$ (blue), *s*-$BCP_{95\%}$_$TBCP_{5\%}$ (red), *s*-$BCP_{90\%}$_$TBCP_{10\%}$ (green) and *s*-$BCP_{84\%}$_$TBCP_{16\%}$ (purple) with increasing content in pre-formed triblock copolymer in the samples.

## 2. Analysis of *s*-P(*n*BA-*co*-S)-SG1 and TBCP by size exclusion chromatography in THF

a)

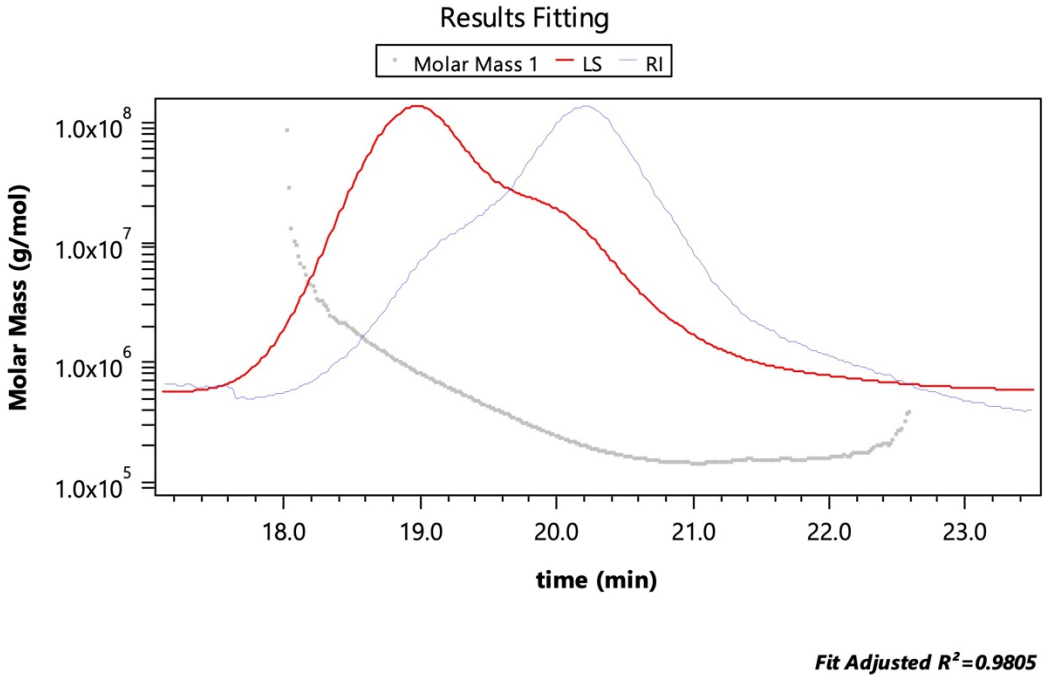


b)

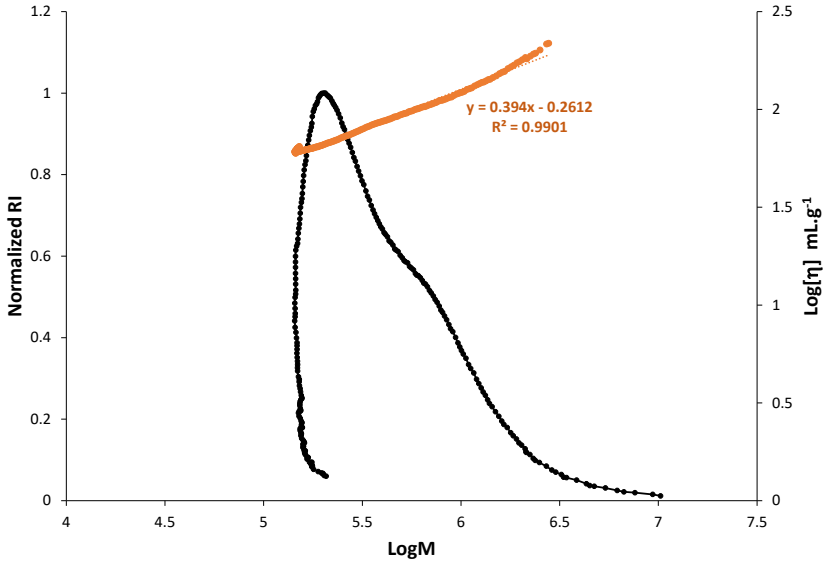


**Figure S4**. SEC chromatograms of *s*-P(*n*BA-*co*-S)-SG1 star macroalkoxyamine. (a) Raw data from Astra software. The plain red line corresponds to LS signal at angle of 90°, blue dotted line to refractive index signal and grey square plot corresponds to molar mass versus elution time. (b) Overlay of RI signal versus LogM (black dots) and Logarithmic intrinsic viscosity ([η]) versus LogM (orange squared plots). The slope, $\alpha = 0.394$, corresponds to Mark-Houwink Sakurada exponent.

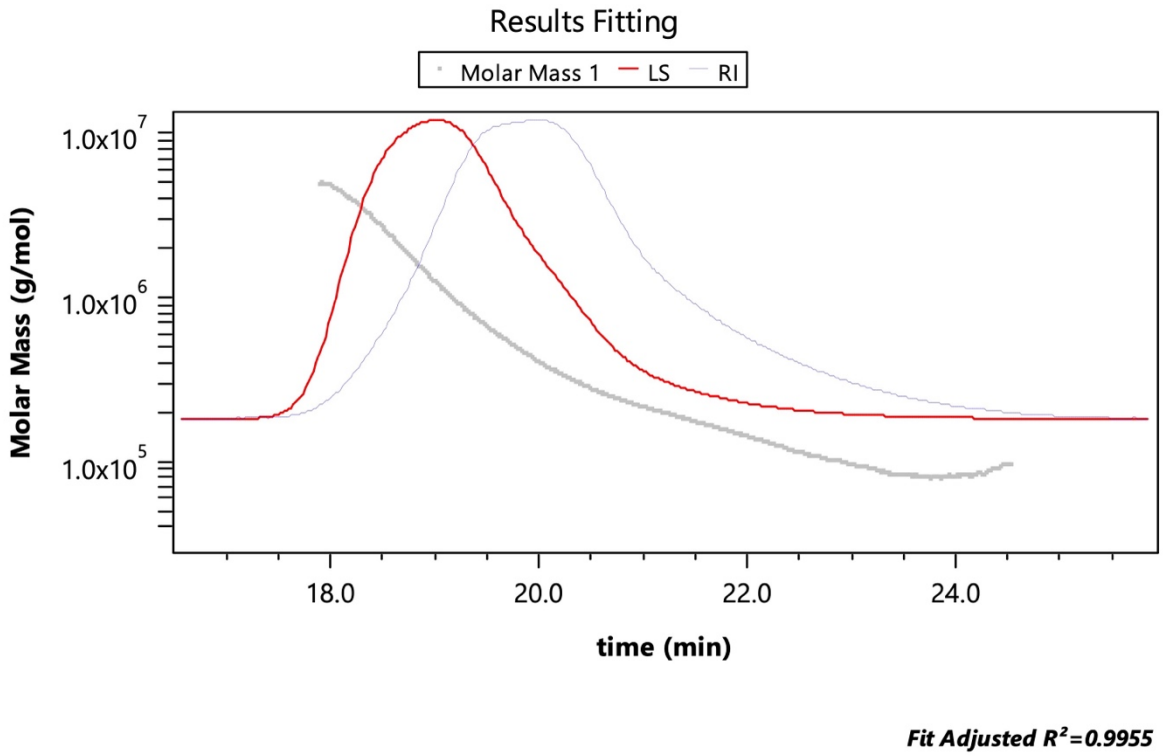


**Figure S5.** SEC chromatograms TBCP. The plain red line corresponds to LS signal at angle of 90°, blue dotted line to refractive index signal and grey square plot corresponds molar mass versus elution time.

## 3. Refractive index increment (*dn/dC*) of *s*-P(*n*BA-*co*-S)-SG1 and TBCP

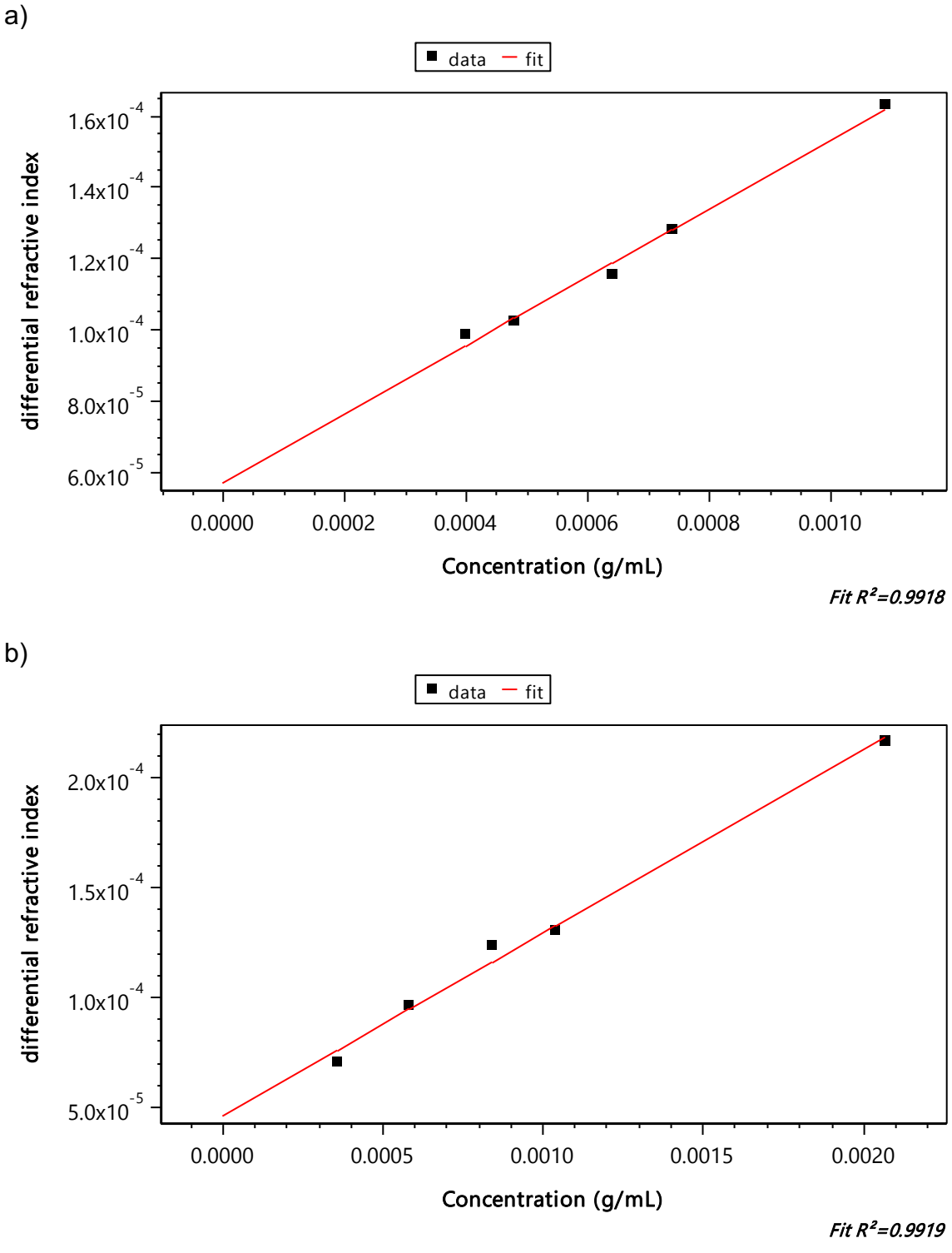


**Figure S6**. Determination of the refractive index increment (*dn/dC*) in THF at 30 °C from the slope of the differential refractive index versus polymer concentration. (a) *s*-P(*n*BA-*co*-S)-SG1 (*dn/dC* = 0.096), (b) TBCP (*dn/dC* = 0.082).

For the series of *s*-BCP_TBCP samples synthesized by PIMS process (Table 1 of main manuscript), the average values of *dn/dC* of the final sample were calculated from the individual weight fraction of each polymer moiety ($W_x$, see Eq S1 and Eq S3) and from the values of *dn/dC* of each homopolymer in THF at 30 °C ($(dn/dC)_{PMMA}$ = 0.090, $(dn/dC)_{PS}$ = 0.185, $(dn/dC)_{PnBA}$ = 0.072).[1]

$$\left(\frac{dn}{dC}\right)_{s-\text{BCPx\%\_TBCPy\%}} = W_{PMMA} \times \left(\frac{dn}{dC}\right)_{PMMA} + W_{PS} \times \left(\frac{dn}{dC}\right)_{PS} + W_{PnBA} \times \left(\frac{dn}{dC}\right)_{PnBA} \quad \textbf{Eq S3.}$$

## 4. Differential scanning calorimetry of *s*-P(*n*BA-*co*-S)-SG1 and *s*-BCP

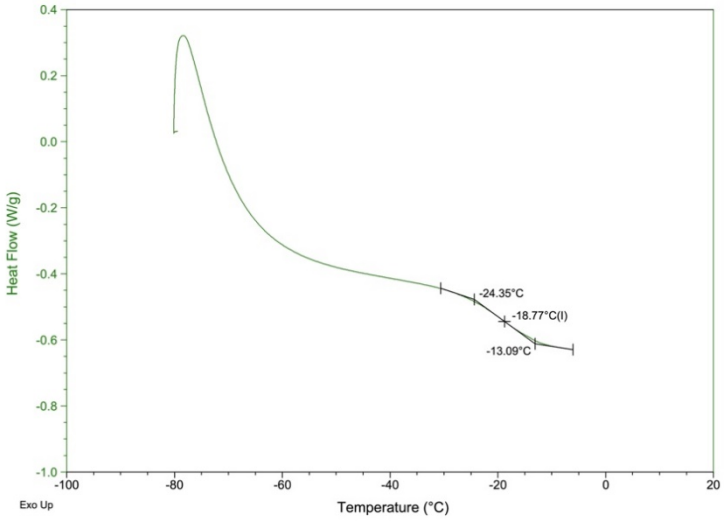


**Figure S7.** DSC trace measured on *s*-P(*n*BA-*co*-S)-SG1 macroalkoxyamine ramped from -85 to 0 °C at 30 °C $min^{-1}$. The sample was first equilibrated at 0 °C, then ramped, 10 °C.$min^{-1}$, down to -85 °C and finally ramped, 30 °C $min^{-1}$, up to 0 °C.

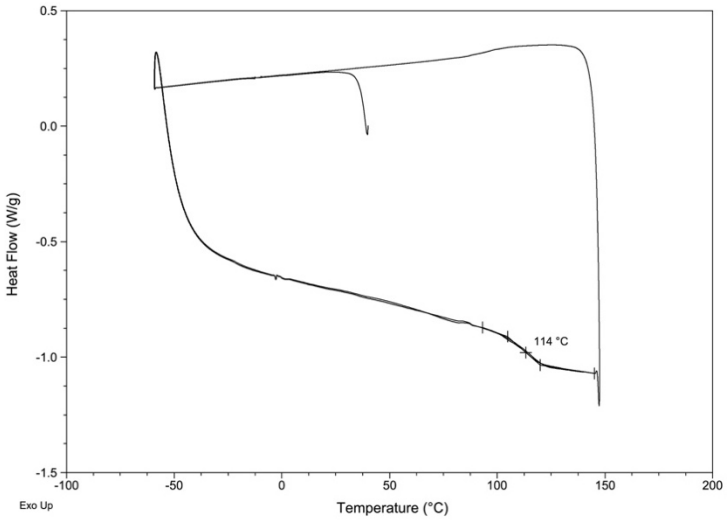


**Figure S8.** DSC traces measured on sample *s*-BCP. Two cycles were performed, with a first a ramp down to -60 °C at 10 °C $min^{-1}$ followed by a ramp up to 150 °C at 30 °C $min^{-1}$.

From Figure S7, the *Tg* of the *s*-P(*n*BA-*co*-S)-SG1 macroalkoxyamine is evaluated at about -19 °C. On Figure S8, the two successive ramps-up are fully superimposed, demonstrating that the sample do not evolve when exposed at 150 °C. It can be noted that the P(*n*BA-*co*-S) block *Tg* is not observed, most probably due to its low amount (7.5 wt-%). On the other hand, the *Tg* of the PMMA block is well marked and evaluated at 114 °C.

## 5. Preparation of PIMS formulations and monomer conversions

**Table S1.** Initial formulation used for PIMS: mass of each component and ratio of MMA monomer over macroalkoxyamine.

| Sample | $m_{s\text{-P}(n\text{BA-}co\text{-S})\text{-SG1}}$ (g) | $m_{\text{MMA}}$ (g) | $m_{\text{TBCP}}$ (g) | $m_{\text{Tinuvin}}$ (g) | $m_{\text{VAZO-88}}$ (g) | $\frac{m_{\text{MMA}}}{m_{s\text{-P}(n\text{BA-}co\text{-S})\text{-SG1}}}$ |
|---|---|---|---|---|---|---|
| *s*-BCP | 15.0 | 184.6 | 0 | 0.20 | 0.14 | 12.3 |
| *s*-BCP$_{97.5\%}$_TBCP$_{2.5\%}$ | 14.6 | 180.0 | 5 | 0.19 | 0.13 | 12.3 |
| *s*-BCP$_{95\%}$_TBCP$_{5\%}$ | 14.2 | 174.4 | 10 | 0.19 | 0.13 | 12.3 |
| *s*-BCP$_{90\%}$_TBCP$_{10\%}$ | 13.5 | 166.2 | 20 | 0.18 | 0.12 | 12.3 |
| *s*-BCP$_{84\%}$_TBCP$_{16\%}$ | 8.2 | 100.8 | 21 | 0.11 | 0.07 | 12.3 |

**Table S2.** Values of residual MMA monomer fraction in the final sample ($F_M$) and MMA conversion ($x_M$).

| Sample | $F_M$ [a] | $x_M$ [b] |
|---|---|---|
| *s*-BCP | 1.3 | 0.995 |
| *s*-BCP$_{97.5\%}$_TBCP$_{2.5\%}$ | 1.2 | 0.991 |
| *s*-BCP$_{95\%}$_TBCP$_{5\%}$ | 1.2 | 0.991 |
| *s*-BCP$_{90\%}$_TBCP$_{10\%}$ | 3.0 | 0.976 |
| *s*-BCP$_{84\%}$_TBCP$_{16\%}$ | 3.9 | 0.968 |

[a] The molar fraction of residual MMA monomer in the sample was calculated from Eq S4.
[b] The MMA conversion was calculated according to Eq S5 by using 1H NMR integrals of MMA and PMMA.

Molar fraction in MMA in the overall polymerized sample:

$$F_M = 1 - \frac{I_M}{I_M + I_x + I_y + I_z} \qquad \textbf{Eq S4.}$$

MMA conversion:

$$x_M = \frac{I_M}{I_M + I_x} \qquad \textbf{Eq S5.}$$

$I_M = (I_{5.5-6.4\ ppm})/2$ is the integral of one proton of vinylic proton of MMA monomer, $I_x = (I_{3.1-3.7\ ppm})/3$ is the integral of one proton of methoxy group of PMMA, $I_y = (I_{6.5-7.2\ ppm})/5$ the integral of one proton of aromatic group of PS and $I_z = (I_{3.3-4.2\ ppm})/2$ the integral of one proton of methylene group of P*n*BA.

## 6. PIMS temperature ramp

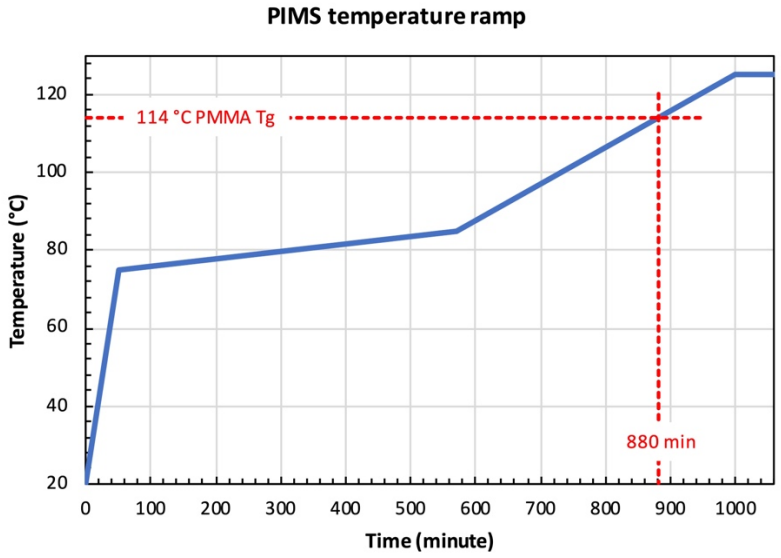


**Figure S9.** Optimized PIMS temperature ramp.[2] The samples are exposed to temperatures below PMMA *Tg* (114 °C) during the first 880 minutes of the process then 180 minutes to higher temperatures.

## 7. Morphological characterization of TBCP

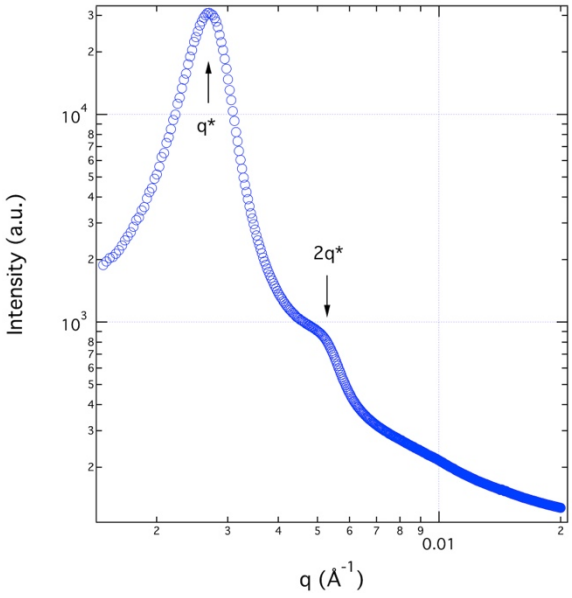


**Figure S10.** SAXS data collected on TBCP after a slow evaporation from toluene solution at room temperature followed by a thermal annealing at 120 °C during 12 hours.

## 8. Transparency of *s*-BCP sample

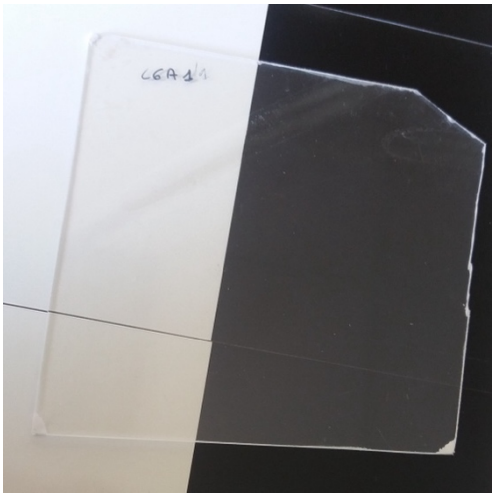

**Figure S11.** Picture of *s*-BCP sample demonstrating its transparency. The dimension of the sample is about 15 cm × 15 cm.

## 9. Overlay of *s*-P(*n*BA-*co*-S)-SG1 and *s*-BCP chromatograms

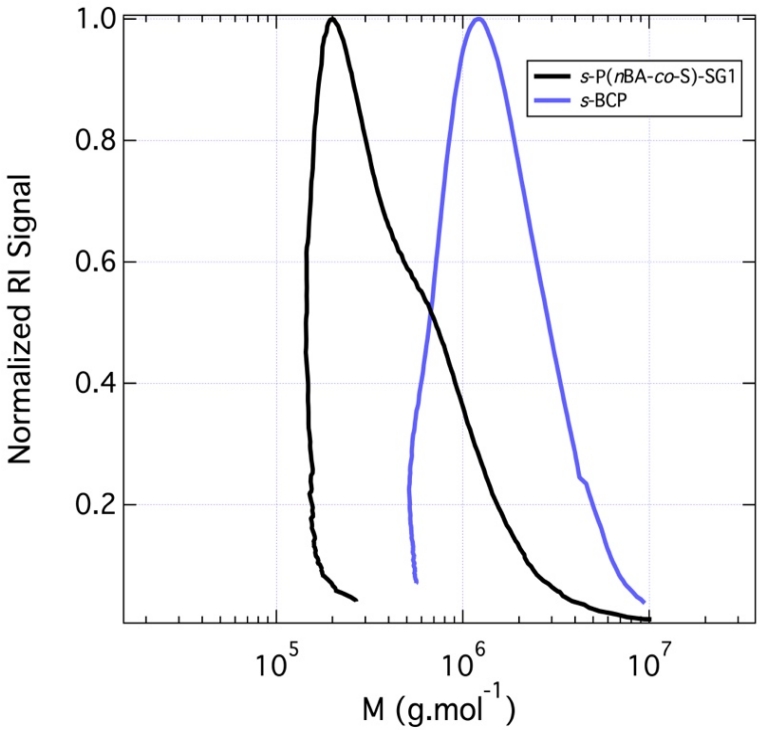


**Figure S12.** Overlay of SEC chromatograms, normalized RI signal versus molar mass, of *s*-P(*n*BA-*co*-S)-SG1 macroinitiator (black) and *s*-BCP (blue).

## 10. Impact of macroalkoxyamine functionality

Monofunctional P(*n*BA-*co*-S)-SG1 and difunctional SG1-P(*n*BA-*co*-S)-SG1 macroalkoxyamines were synthesized by NMP to perform a preliminary screening of PIMS morphology. Both macroalkoxyamine features are presented in Table S3. The primary objective was to approach $M_n$ ratios of 2/3 and 1/3 compared to the *s*-P(*n*BA-*co*-S)-SG1 trifunctional macroalkoxyamine for respectively the difunctional and monofunctional macroalkoxyamine, in order to achieve equivalent branch $M_n$. The PIMS samples were prepared similarly to the ones using the star *s*-P(*n*BA-*co*-S)-SG1, see experimental part and Table S4.

**Table S3.** Macromolecular features of additional macroalkoxyamine (macro-SG1).

| | **Macro-SG1 functionality** | **Styrene (wt-%)[a]** | **$M_n$ (g mol$^{-1}$) [b]** | **$Đ$ [b]** |
|---|---|---|---|---|
| SG1-P(*n*BA-*co*-S)-SG1 | 2 | 19 | $8.7 \times 10^4$ | 1.2 |
| P(*n*BA-*co*-S)-SG1 | 1 | 20 | $3.8 \times 10^4$ | 1.1 |

[a] Weight fraction of styrene in the P(*n*BA-*co*-S) copolymer calculated from EqS1 from $^1$H NMR spectra.
[b] Number-average molar mass and dispersity obtained by SEC MALLS.

**Table S4.** Formulation compositions and macromolecular features of PIMS samples produced from monofunctional and difunctional macroalkoxyamine from Table S3.

| **Formulations** | | **PIMS samples** | | | | |
|---|---|---|---|---|---|---|
| **Macro-SG1 functionality** | **Macro-SG1 (wt-%)** | **BCP structure** | **$M_n$ (g mol$^{-1}$) [a]** | **$Đ$ [a]** | **P(*n*BA-*co*-S) (wt-%) [b]** | **PMMA (wt-%) [b]** |
| 2 | 7.5 | AB | $9.5 \times 10^5$ | 1.1 | 12.1 | 86.6 |
| 1 | 7.5 | BAB | $4.6 \times 10^5$ | 1.7 | 10.3 | 87 |

[a] Number-average molar mass and dispersity obtained by SEC MALLS.
[b] Weight fraction determined by Eq S1 from NMR spectra; the wt-% to 100 corresponds to residual MMA.

Topographic AFM images collected on the ultramicrotomed PIMS samples are presented in Figure S13. Sample prepared from monofunctional macroalkoxyamine (Figure S13a) present a microphase separation, with dark P(*n*BA-*co*-S) spherical domains dispersed in a bright PMMA majority phase. The spherical domains present diameter ranging from 30 to 70 nm, with sphere-to-sphere distances ranging between 100 and 300 nm. Sample prepared from the difunctional macroalkoxyamine (Figure S13b) presents heterogeneities at large length scale.

Nonetheless, one can discern spherical nano-domains of P(*n*BA-*co*-S) with diameters ranging between 30 and 60 nm and sphere-to-sphere distances ranging from 100 to 200 nm.

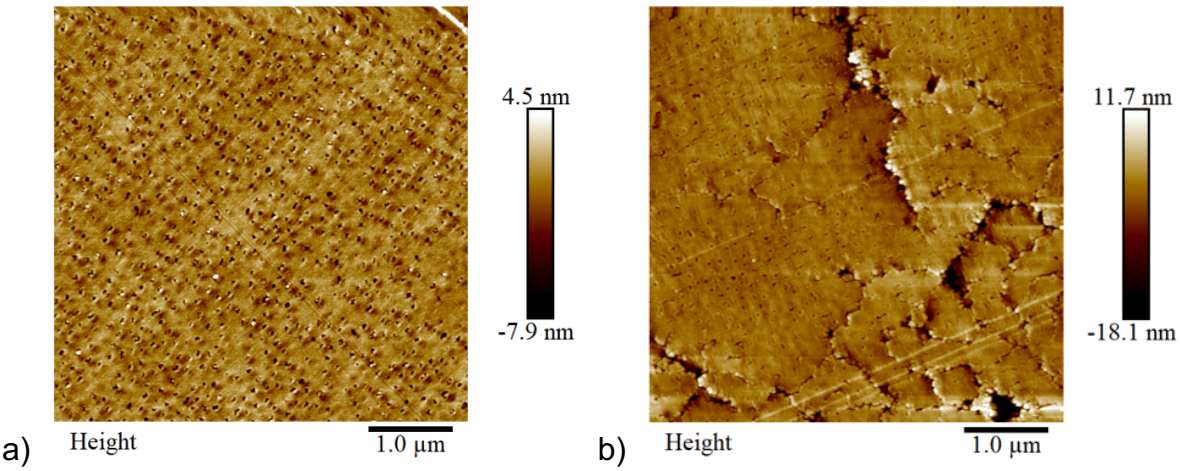


**Figure S13.** AFM height images collected on PIMS samples prepared from formulations containing a) 7.5 wt-% of monofunctional macro-SG1 in MMA, and b) 7.5 wt-% difunctional macro-SG1 in MMA.

## 11. Impact of *s*-P(*n*BA-*co*-S)-SG1 content in the formulation

To evaluate the influence of macroalkoxyamine content in the formulations, additional ratios of *s*-P(*n*BA-*co*-S)-SG1 were investigated, i.e., 3.5 and 15 wt-%. The PIMS samples were prepared similarly to the ones with 7.5 wt-% of *s*-P(*n*BA-*co*-S)-SG1 star macroalkoxyamine, see experimental part and Table S5.

**Table S5.** Initial resins and macromolecular features of PIMS samples prepared from *s*-P(*n*BA-*co*-S)-SG1 star macroalkoxyamine.

| **Formulations** | **PIMS samples** | | | | |
|---|---|---|---|---|---|
| ***s*-P(*n*BA-*co*-S)-SG1 (wt-%)** | **BCP structure** | **$M_n$ (g mol$^{-1}$) [a]** | **$Đ$ [a]** | **P(*n*BA-*co*-S) (wt-%) [b]** | **PMMA (wt-%) [b]** |
| 3.5 | *s*-(AB)$_3$ | $1.5 \times 10^6$ | 1.4 | 5.7 | 92.9 |
| 15 | *s*-(AB)$_3$ | $8.2 \times 10^5$ | 1.6 | 13.5 | 85.1 |

[a] Number-average molar mass and dispersity obtained by SEC MALLS.
[b] Weight fraction determined by Eq S1 from NMR spectra, the wt-% to 100 corresponds to residual MMA.

Topographic AFM images collected on the ultramicrotomed PIMS samples are presented in Figure S14. The sample prepared with 3.5 wt-% of macroalkoxyamine displays dispersed P(*n*BA-*co*-S) spherical domains of 55 ±5 nm in diameter, as well as elongated objects with similar lateral dimension (Figure S14a). When the macroalkoxyamine content is increased up

to 15 wt-% the morphology evolves drastically to a polygonal-like structure, with PMMA polygons separated by a thin layer of P(*n*BA-*co*-S) (Figure S14b). The polygon averaged diameter ranges from 200 to 400 nm and the P(*n*BA-*co*-S) layer thickness ranges from 40 to 80 nm. The observed morphologies evolve drastically with macroalkoxyamine content. Only, the 7.5 wt-% of macroalkoxyamine reveals the targeted LAM structure (Figure 1).

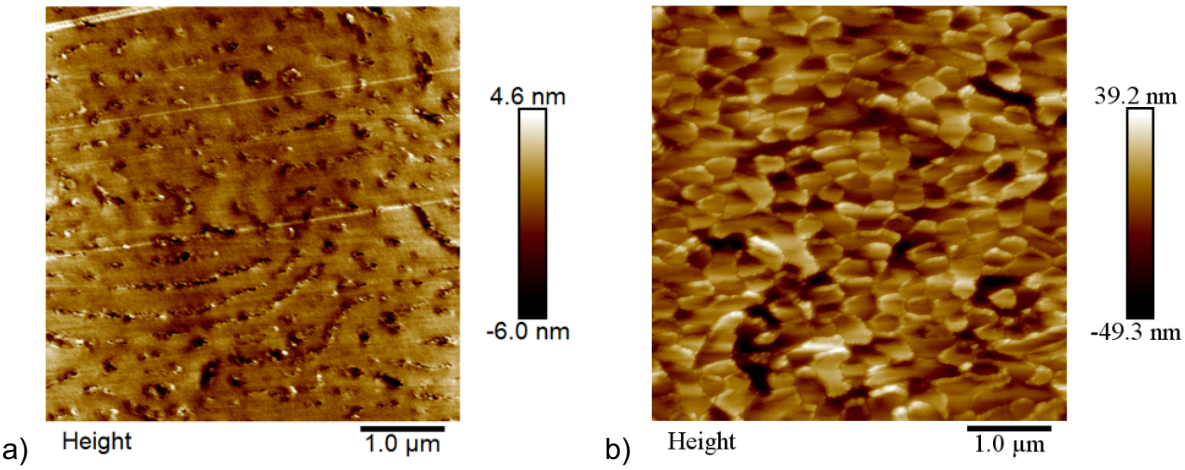


**Figure S14.** AFM height images collected on PIMS samples prepared from resins containing various fraction of star macroalkoxyamine: a) 3.5 wt-% of *s*-P(*n*BA-*co*-S)-SG1 in MMA, and b) 15 wt-% of *s*-P(*n*BA-*co*-S)-SG1 in MMA.

## 12. Analysis of *s*-BCP_TBCP samples by size exclusion chromatography in THF

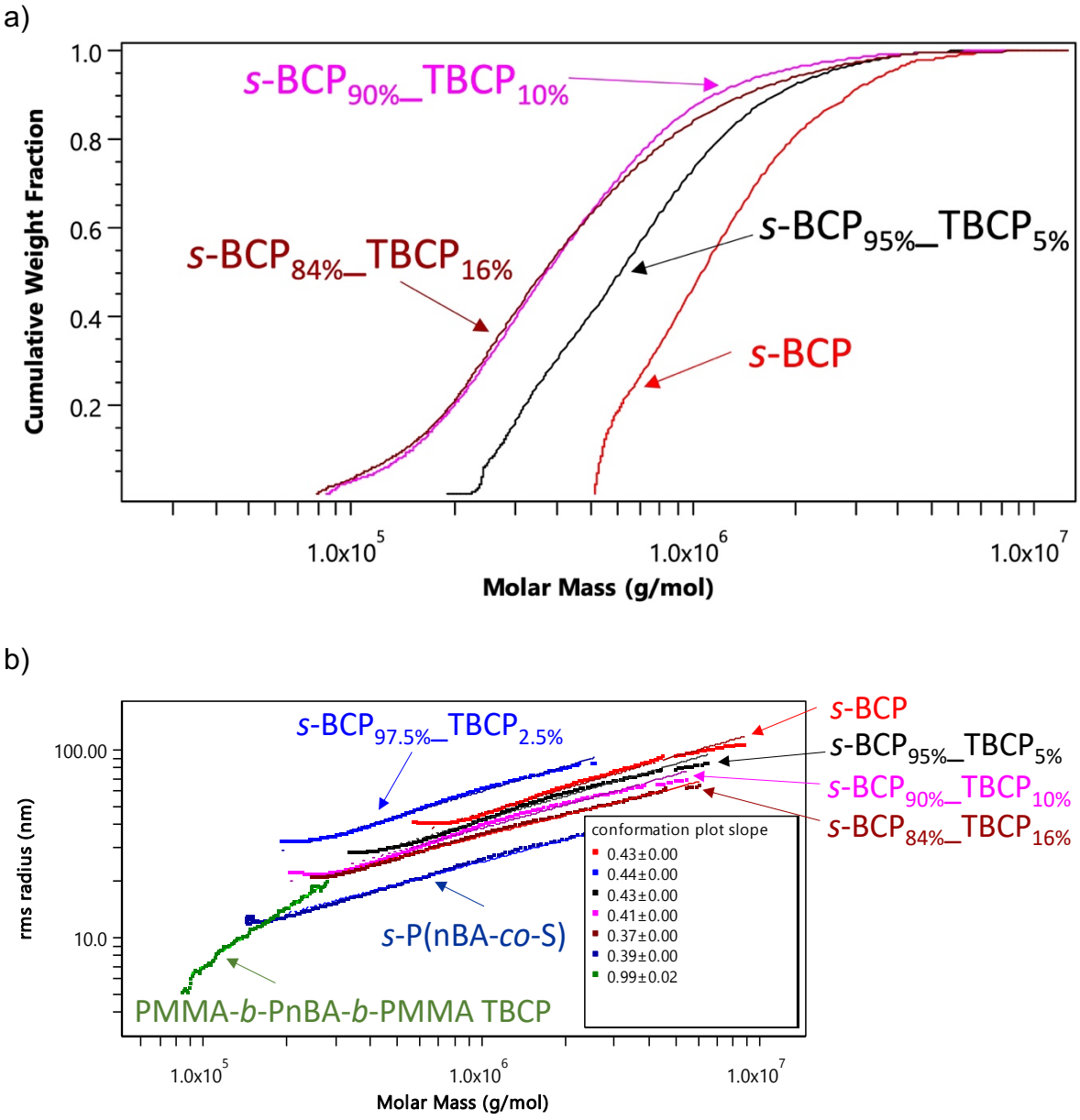


**Figure S15.** SEC analysis of samples prepared by PIMS: a) Cumulative weight fraction versus molar mass, b) Conformation plot (gyration radius versus molar mass $R_g \propto M^{\alpha}$ with $\alpha = 0.37$ to 0.44 for *s*-BCP and *s*-BCP_TBCP samples synthesized by PIMS.

The slope of the conformation plot ($\alpha$ exponent) of linear random coils are typically 0.58–0.60. The decrease of the slope to lower values indicates a more compact macromolecular structure, usually due to the presence of branched macromolecules.[3]

**Table S6.** *s*-BCP and *s*-BCP_TBCP samples compositions and their respective arm number-average molar mass.

| Samples | $m_{s\text{-BCP}}$ [a] | $m_{TBCP}$ [a] | $x_{s\text{-BCP}}$ [b] | $x_{TBCP}$ [b] | $M_{n\_exp}$ [c] (g mol$^{-1}$) | $M_{n\_theo}$ [d] (g mol$^{-1}$) | $M_{n\_exp\ arm}$ [e] (g mol$^{-1}$) |
|---|---|---|---|---|---|---|---|
| *s*-BCP | 1 | 0 | 1.0 | 0.0 | $9.83 \times 10^5$ | $9.83 \times 10^5$ | $3.28 \times 10^5$ |
| *s*-BCP$_{97.5\%}$_TBCP$_{2.5\%}$ | 0.975 | 0.025 | 0.67 | 0.33 | $6.68 \times 10^5$ | $6.74 \times 10^5$ | $2.25 \times 10^5$ |
| *s*-BCP$_{95\%}$_TBCP$_{5\%}$ | 0.95 | 0.05 | 0.5 | 0.5 | $5.30 \times 10^5$ | $5.13 \times 10^5$ | $1.81 \times 10^5$ |
| *s*-BCP$_{90\%}$_TBCP$_{10\%}$ | 0.9 | 0.1 | 0.32 | 0.68 | $3.02 \times 10^5$ | $3.47 \times 10^5$ | $1.07 \times 10^5$ |
| *s*-BCP$_{84\%}$_TBCP$_{16\%}$ | 0.84 | 0.16 | 0.21 | 0.79 | $2.92 \times 10^5$ | $2.50 \times 10^5$ | $1.04 \times 10^5$ |
| TBCP | 0 | 1 | 0 | 1 | $5.09 \times 10^4$ | $5.09 \times 10^4$ | $2.54 \times 10^4$ |

[a] $m_{s\text{-BCP}}$ and $m_{TBCP}$ are respectively the initial weight fractions of the *s*-BCP and TBCP in each sample.
[b] $x_{s\text{-BCP}}$ and $x_{TBCP}$ are the estimated molar fractions of respectively *s*-BCP and TBCP in the samples calculated from Eq S6 and Eq S7.
[c] Experimental number-average molar mass of the copolymer mixture determined by SEC (see Figure 2f).
[d] Theoretical number-average molar mass of the copolymer mixture calculated from the molar fractions of *s*-BCP and TBCP (Eq S8).
[e] Experimental $M_n$ of each P(*n*BA-*co*-S)-*b*-PMMA arm calculated from Eq S9 considering 2 arms for the TBCP and 3 for the *s*-BCP.

$$x_{s\text{-BCP}} = n_{BCP} / (n_{BCP} + n_{TBCP}) = 1 / [\ 1 + (m_{TBCP} \times M_{n\_s\text{-BCP}}) / (m_{s\text{-BCP}} \times M_{n\_TBCP})] \qquad \textbf{Eq S6.}$$

with $M_{n\_s\text{-BCP}}$ and $M_{n\_TBCP}$ the experimental number-average molar mass of respectively *s*-BCP ($M_n = 9.83 \times 10^5$ g mol$^{-1}$) and TBCP ($M_n = 5.9 \times 10^4$ g mol$^{-1}$) determined by SEC-MALLS.

$$x_{TBCP} = 1 - x_{s\text{-BCP}} \qquad \textbf{Eq S7.}$$

$$M_{n\_theo} = x_{s\text{-BCP}} \times M_{n\_s\text{-BCP}} + x_{TBCP} \times M_{n\_TBCP} \qquad \textbf{Eq S8.}$$

$$M_{n\_exp\ arm} = x_{s\text{-BCP}} \times M_{n\_s\text{-BCP}} / 3 + x_{TBCP} \times M_{n\_TBCP} / 2 \qquad \textbf{Eq S9.}$$

## 13. Rheological properties of *s*-BCP and *s*-BCP_TBCP samples

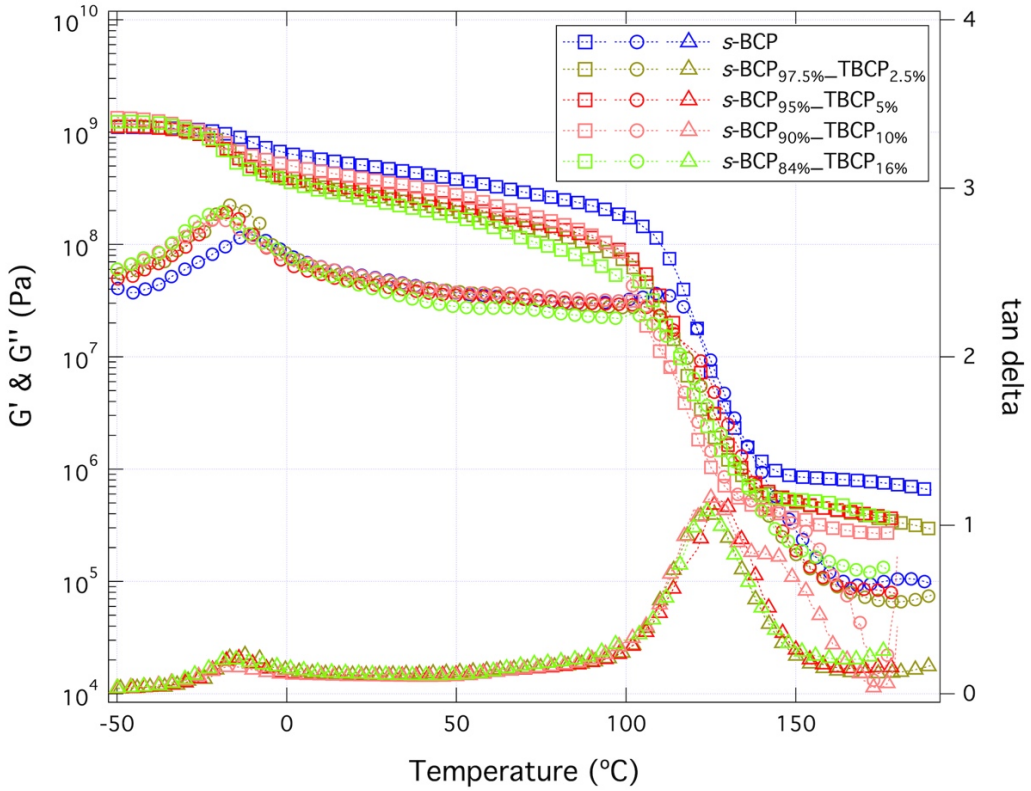


**Figure S16.** Thermomechanical analysis realized at 1 Hz and 1 C $min^{-1}$ for *s*-BCP and *s*-BCP_TBCP samples. The $G'$ curves are represented with open squares (☐), $G''$ with open circles (○) and $tan\delta$ with open triangles (△).

Rheological properties were investigated by dynamical mechanical thermal analysis (Figure S10). The storage ($G'$) and loss ($G''$) moduli global behavior are rather similar for all samples, independently on TBCP content. The $tan\delta$ curves display two peaks. The first one, presenting a moderate intensity, appears at low temperatures between -20 and -10 °C and a second, more intense, between 120 and 130 °C. The presence of those two well distinct peaks confirms that the samples are phase separated. Indeed, those peaks are the signatures of both block dynamics, pointing out the mechanical glass transition temperatures, $T\alpha$, determined at the maximum of $tan\delta$. $T\alpha$ ranging from -20 to -10 °C is associated to macroinitiator and $T\alpha$ ranging from 120 to 130 °C to the PMMA block. Focusing on $G'$ modulus at the rubbery plateau a decrease is observed with TBCP content, i.e., increasing soft phase content, as expected. Above PMMA glass transition temperature, all samples present a solid-like behavior, storage and loss moduli remain constant and such as the rubbery plateau, also the value of $G'$ decrease with TBCP content.

## REFERENCES

(1) Brandrup, J.; Immergut, E. H.; Grulke, E. A. Polymer Handbook 4th Edition John Wiley & Sons, 2003.

(2) Bourrigaud, S.; Brocas, A.-L.; Cazaumayou, S.; Garcia Andujar, L.; Save, M.; Derail, C.; Rubatat, L. Process for polymerizing a composition in the presence of a block copolymer. WO 2020/240115 A1, 2020.

(3) Podzimek, S. *Light Scattering Size Exclusion Chromatography and Asymmetric Flow Field Flow Fractionation*; A John Wiley & Sons, Inc. , 2011.